


Graceful exit from inflation and reheating with twin waterfall scalar fields

Hyun Min Lee^{*} and Adriana G. Menkara[†]

Department of Physics, Chung-Ang University, Seoul 06974, Republic of Korea

 (Received 24 April 2023; accepted 31 May 2023; published 16 June 2023)

We study hybrid inflation with a pseudo-Nambu-Goldstone boson inflaton and two waterfall scalar fields. The Z_2 symmetry for the waterfall fields keeps the inflaton potential flat against quantum corrections coming from the waterfall couplings, and it is broken spontaneously in the vacuum without a domain-wall problem within the Hubble horizon of our Universe. We show that the Z_2 -invariant Higgs portal couplings to the waterfall fields are responsible for the reheating process, leading to a sufficiently large reheating temperature after inflation. In the presence of an extra Z'_2 symmetry, one of the waterfall fields or another singlet scalar field becomes a dark matter candidate. In particular, we find that preheating is sufficient to account for the correct relic density of the waterfall dark matter.

DOI: [10.1103/PhysRevD.107.115019](https://doi.org/10.1103/PhysRevD.107.115019)

I. INTRODUCTION

Cosmic inflation [1] has been successful for solving various problems in standard big bang cosmology, such as the initial conditions for the Friedman-Lemaître-Robertson-Walker universe (namely, homogeneity, isotropy, and flatness), the inhomogeneities imprinted in the cosmic microwave background (CMB) anisotropies [2,3], and large-scale structures. The period of exponential expansion of the Universe requires a very flat potential of the scalar field, the so-called inflaton, thus accounting for the early vacuum energy domination.

On the other hand, the exponential expansion must end in order to recover the success of big bang cosmology, namely, big bang nucleosynthesis (BBN). Otherwise, the Universe would have continued to undergo the exponential expansion, being left with nothing. This requires the graceful exit from inflation [4] and the reheating process [5]. Thus, we need to specify the interactions between the inflaton and the Standard Model (SM) in order to populate the SM particles in the postinflation regime.

In chaotic inflation models with a single inflaton [4], inflation ends due to the violation of the slow-roll condition, so the graceful exit from inflation is naturally realized. Hybrid inflation [6], on the other hand, requires at least two scalar fields for inflation and the graceful exit at the same time. In this case, the inflaton drives a slow-roll

inflation whereas the graceful exit or the violation of the slow-roll condition is achieved due to the tachyonic instability of another scalar field [7], the so-called waterfall field. It is conceivable to have multiple scalar fields in a UV-complete theory, such as in compactifications of string theory, so hybrid inflation scenarios are more realistic cases and even single-field inflation models can be regarded as a certain limit of decoupling heavy particles.

In this article, we consider a model for hybrid inflation and its reheating dynamics with a pseudo-Nambu-Goldstone boson (pNGB) inflaton and two waterfall scalar fields [8]. In this model, the shift symmetry of the inflaton ensures a naturally flat potential for the inflaton, whereas the Z_2 discrete symmetry for two waterfall fields [8,9] renders the inflaton potential insensitive to loop corrections coming from the couplings between the waterfall fields and the inflaton.

From the post-inflationary dynamics of the hybrid inflation, we discuss the preheating effects in the presence of waterfall-field-dependent masses and the perturbative decay of the waterfall field for reheating. The Z_2 -invariant Higgs portal couplings to the waterfall fields are responsible for reheating. Moreover, focusing on the case that the twin waterfall field or another singlet scalar field coupled to the waterfall field is a stable dark matter candidate due to another Z'_2 symmetry, we also calculate the dark matter abundance from preheating and/or the perturbative decay of the oscillating waterfall field.

The paper is organized as follows. We first present the model setup for hybrid inflation with a pNGB inflaton and two waterfall fields and the condition for the waterfall transition and the robustness of the tree-level inflaton potential in this case. Then, we show the inflationary predictions of the model, the waterfall field dynamics, and the vacuum structure, constraining the parameters of

^{*}hminlee@cau.ac.kr

[†]amenkara@cau.ac.kr

Published by the American Physical Society under the terms of the Creative Commons Attribution 4.0 International license. Further distribution of this work must maintain attribution to the author(s) and the published article's title, journal citation, and DOI. Funded by SCOAP³.

the waterfall sector. Next, we discuss the preheating effects from the waterfall transition and the reheating from the perturbative decay of the waterfall field after preheating. In the presence of an extra Z'_2 symmetry, we regard the twin waterfall field as a dark matter candidate and discuss the preheating and the perturbative decay of the waterfall field for dark matter production. Finally, we draw our conclusions.

II. THE MODEL

We consider a pNGB ϕ as the inflaton and two real scalar fields χ_1, χ_2 as the waterfall fields in the hybrid inflation scenarios [8]. We discuss the roles of discrete symmetries and their origin for the UV-insensitive inflaton potential and the stability of dark matter.

A. Hybrid inflation

We decompose the scalar potential for the hybrid inflation into the following:

$$V(\phi, \chi_1, \chi_2, H) = V_I(\phi) + V_W(\phi, \chi_1, \chi_2) + V_{\text{RH}}(\chi_1, \chi_2, H), \quad (1)$$

where $V_I(\phi)$ is the inflaton potential, $V_W(\phi, \chi_1, \chi_2)$ is the waterfall field part consisting of two waterfall fields, and $V_{\text{RH}}(\chi_1, \chi_2, H)$ is the potential part for reheating the Universe by the couplings of the waterfall fields to the SM Higgs H .

Imposing a Z_2 discrete symmetry [8,9] with

$$Z_2: \phi \rightarrow -\phi, \quad \chi_1 \leftrightarrow \chi_2, \quad (2)$$

we take the scalar potential for the hybrid inflation in the following form:

$$V_I(\phi) = V_0 + A(\phi), \quad (3)$$

$$\begin{aligned} V_W(\phi, \chi_1, \chi_2) = & B(\phi)(\chi_1^2 - \chi_2^2) + \frac{1}{2}m_\chi^2(\chi_1^2 + \chi_2^2) - \alpha^2\chi_1\chi_2 \\ & + \beta(\chi_1^3 + \chi_2^3) + \gamma(\chi_1^2\chi_2 + \chi_1\chi_2^2) \\ & + \frac{1}{4}\lambda_\chi(\chi_1^4 + \chi_2^4) + \frac{1}{2}\bar{\lambda}_\chi\chi_1^2\chi_2^2 \\ & + \frac{1}{3}\lambda'_\chi(\chi_1^3\chi_2 + \chi_1\chi_2^3), \end{aligned} \quad (4)$$

and

$$V_{\text{RH}}(\chi_1, \chi_2, H) = \kappa_1(\chi_1^2 + \chi_2^2)|H|^2 + \kappa_2\chi_1\chi_2|H|^2. \quad (5)$$

Here, V_0 is the constant vacuum energy during inflation, and $A(\phi), B(\phi)$ are arbitrary functions of ϕ , satisfying $A(-\phi) = A(\phi)$ and $B(-\phi) = -B(\phi)$. The simple choices for $A(\phi), B(\phi)$ are $A(\phi) = -\frac{1}{2}m_\phi^2\phi^2$ and $B(\phi) = -g\phi$.

The renormalizable waterfall field couplings, $\phi^2(\chi_1^2 + \chi_2^2)$, can also be introduced, being consistent with the Z_2 symmetry and contributing to the effective masses for the waterfall fields during inflation. But, as will be shown below, the shift symmetry for ϕ makes such higher-order terms in ϕ naturally suppressed.

In the presence of a separate Z'_2 symmetry acting only on χ_2 ,

$$Z'_2: \phi \rightarrow \phi, \quad \chi_1 \rightarrow \chi_1, \quad \chi_2 \rightarrow -\chi_2, \quad (6)$$

we can set $\alpha = \beta = \gamma = \lambda'_\chi = 0$ in combination with the Z_2 symmetry, and $\kappa_2 = 0$, so χ_2 can be a candidate for dark matter. In this case, the independent parameters of the waterfall fields are reduced to $\lambda_\chi, \bar{\lambda}_\chi$, and κ_1 only.

For the concrete discussion on inflation and the waterfall transition, in the later analysis we take the inflaton potential in Eq. (3) and the waterfall field couplings for the inflaton in Eq. (4) in the following periodic forms [8]:

$$A(\phi) = \Lambda^4 \cos\left(\frac{\phi}{f}\right), \quad (7)$$

$$B(\phi) = -\frac{1}{2}\mu^2 \sin\left(\frac{\phi}{2f}\right). \quad (8)$$

Then, the shift symmetry for ϕ is broken into a discrete one, $\phi \rightarrow \phi + 4\pi f$. Expanding the sinuous functions around the origin, we can have $A(\phi) \simeq \Lambda^4 - \frac{1}{2}m_\phi^2\phi^2$ with $m_\phi^2 = \frac{\Lambda^4}{f^2}$ and $B(\phi) \simeq -g\phi$ with $g = \frac{\mu^2}{4f}$. For hybrid inflation, we need to choose $V_0 \gtrsim \Lambda^4$, so the graceful exit from inflation is possible due to the transition with waterfall fields.

We first identify the inflaton-dependent mass eigenvalues for the waterfall fields as

$$m_1^2(\phi) = m_\chi^2 - \sqrt{4B^2(\phi) + \alpha^4}, \quad (9)$$

$$m_2^2(\phi) = m_\chi^2 + \sqrt{4B^2(\phi) + \alpha^4}, \quad (10)$$

and the mixing angle θ between the waterfall fields depends on the inflaton field as

$$\sin 2\theta(\phi) = \frac{2\alpha^2}{m_2^2(\phi) - m_1^2(\phi)}. \quad (11)$$

Here we can keep the kinetic terms for the waterfall fields in the approximately canonical forms during the slow-roll inflation. For $\alpha = 0$, there is no mixing between the waterfall fields, so we can just keep track of the waterfall field χ_1 to determine the end of inflation.

During inflation, there is no vacuum expectation value (VEV) for the waterfall fields for $m_1^2(\phi) > 0$ and $m_2^2(\phi) > 0$, namely, for $\phi < \phi_c$ where ϕ_c satisfies $B^2(\phi_c) = m_\chi^4 - \alpha^4$

with $\alpha < m_\chi$ and $B(\phi)$ is a monotonically increasing function of ϕ near ϕ_c , so slow-roll inflation takes place. For instance, from Eq. (9) with Eq. (8), and setting $m_1^2(\phi_c) = 0$, we find the point of the waterfall transition ϕ_c as

$$\phi_c = 2f \arcsin\left(\sqrt{m_\chi^4 - \alpha^4/\mu^2}\right), \quad (12)$$

with $\sqrt{m_\chi^4 - \alpha^4} < \mu^2$ and $\alpha < m_\chi$. Then, the waterfall fields are heavy enough for $\mu, m_\chi \gg H_I$, with H_I being the Hubble scale during inflation, so we can describe the slow-roll inflation by the inflaton potential given in Eq. (3) with Eq. (7). At $\phi = \phi_c$ the waterfall field with mass m_1 starts to become unstable, ending inflation even if the slow-roll condition for the inflaton direction is not violated.

B. UV-insensitive inflaton potential

The couplings of the waterfall fields to the inflaton give rise to the corrections to the inflaton potential. As the waterfall fields have masses much heavier than the Hubble scale during inflation and they couple to the inflaton for the waterfall transition, it is important to perform a consistency check of the waterfall field couplings for inflation.

The waterfall field couplings to the one-loop Coleman-Weinberg potential for the inflaton in the cutoff regularization with a cutoff scale M_* are as follows:

$$\begin{aligned} V_{\text{CW}} &= \frac{1}{64\pi^2} \sum_{i=1,2} \left[2m_{\chi_i}^2 M_*^2 - m_{\chi_i}^4 \ln\left(\frac{e^{\frac{1}{2}} M_*^2}{m_{\chi_i}^2}\right) \right] \\ &\simeq \frac{1}{16\pi^2} m_\chi^2 M_*^2 - \frac{1}{64\pi^2} (m_\chi^4 + 4B^2(\phi) + \alpha^4) \ln \frac{M_*^2}{m_\chi^2}. \end{aligned} \quad (13)$$

Here, a constant vacuum energy proportional to M_*^2 must be renormalized to get the desirable inflation energy. But, we find that the quadratically divergent part of the inflaton potential is canceled between the waterfall fields due to the Z_2 discrete symmetry. On the other hand, there remain the logarithmically divergent terms of the inflaton potential, which can be ignored during inflation as long as $B^2(\phi) \lesssim 16\pi^2 |A(\phi)|$ is satisfied. For instance, for the periodic forms given in Eqs. (7) and (8), we can set the bound on the loop corrections as $\mu^2 \lesssim 8\pi\Lambda^2$.

C. Origin of discrete symmetries

We comment on the origin of the discrete symmetries for the inflaton and the waterfall fields. Suppose that a $U(1)$ global symmetry is broken to a Z_4 symmetry, under which the inflaton ϕ and a complex scalar field Φ transform by

$$Z_4: \phi \rightarrow \phi, \quad \Phi \rightarrow -i\Phi. \quad (14)$$

Moreover, we take the CP symmetry in the dark sector as

$$CP: \phi \rightarrow -\phi, \quad \Phi \rightarrow \Phi^*. \quad (15)$$

As a result of combining $Z_4 \times CP$, we get

$$Z_4 \times CP: \phi \rightarrow -\phi, \quad \Phi \rightarrow i\Phi^*. \quad (16)$$

In this case, writing $\Phi = \frac{1}{\sqrt{2}}(\chi_1 + i\chi_2)$, we can realize $\phi \rightarrow -\phi$ and $\chi_1 \leftrightarrow \chi_2$ under $Z_4 \times CP$, as required for the Z_2 symmetry, thus providing the potential for hybrid inflation in our model. On the other hand, the separate Z_2' symmetry for χ_2 corresponds to

$$Z_2': \phi \rightarrow \phi, \quad \Phi \rightarrow \Phi^*. \quad (17)$$

III. INFLATION AND WATERFALL FIELD DYNAMICS

We now discuss the inflationary predictions of the pNGB inflation with twin waterfall fields. Ignoring the classical dynamics of the waterfall fields during inflation, we focus on slow-roll inflation and the condition for the waterfall transition. Then, we show how the vacuum structure is connected to the inflation regime, constraining the waterfall sector parameters.

A. Inflationary predictions

From the inflaton potential given in Eq. (7), we first obtain the slow-roll parameters for inflation as

$$\epsilon = \frac{M_P^2 \Lambda^8 \sin^2(\phi/f)}{2f^2 (V_0 + \Lambda^4 \cos(\phi/f))^2}, \quad (18)$$

$$\eta = -\frac{M_P^2 \Lambda^4 \cos(\phi/f)}{f^2 (V_0 + \Lambda^4 \cos(\phi/f))}. \quad (19)$$

The number of e -foldings is also obtained as

$$\begin{aligned} N &= \frac{1}{M_P} \int_{\phi_*}^{\phi_c} \frac{1}{\sqrt{2\epsilon}} d\phi \\ &= \frac{f^2}{2M_P^2 \Lambda^4} \left[V_0 \ln\left(\tan^2\left(\frac{\phi_c}{2f}\right)\right) + \Lambda^4 \ln\left(\sin^2\left(\frac{\phi_c}{f}\right)\right) \right] \\ &\quad - (\phi_c \rightarrow \phi_*), \end{aligned} \quad (20)$$

where ϕ_* , ϕ_c are the inflaton field values at the horizon exit and at the end of inflation, respectively.

For $V_0 \gg \Lambda^4$ for hybrid inflation, the slow-roll parameters and the number of e -foldings are approximated [8] as

$$\eta_* \simeq -\frac{M_P^2 \Lambda^4}{f^2 V_0} \cos(\phi_*/f), \quad (21)$$

$$\epsilon_* \simeq \frac{M_P^2 \Lambda^8}{2f^2 V_0^2} \sin^2(\phi_*/f), \quad (22)$$

$$N \simeq \frac{f^2 V_0}{M_P^2 \Lambda^4} \ln \left(\frac{\tan(\phi_c/(2f))}{\tan(\phi_*/(2f))} \right). \quad (23)$$

As a result, the spectral index and the tensor-to-scalar ratio can be determined by

$$n_s = 1 + 2\eta_* - 6\epsilon_*, \quad (24)$$

$$r = 16\epsilon_*. \quad (25)$$

The CMB normalization, $A_s = \frac{1}{24\pi^2} \frac{V_0 + \Lambda^4}{\epsilon_* M_P^4} \simeq 2.1 \times 10^{-9}$, leads to

$$r = 3.2 \times 10^7 \cdot \frac{V_0}{M_P^4}. \quad (26)$$

The observed spectral index from *Planck* data, $n_s = 0.967 \pm 0.0037$ [2], sets $2\eta_* \simeq -0.0033$, because $\epsilon_* \ll |\eta_*|$ in our case. We note that the critical value ϕ_c of the inflaton should satisfy $\phi_* \lesssim \phi_c \lesssim f$ for the number of e -foldings, $N = 50$ – 60 , to solve the horizon problem. Moreover, from the *Planck* bound on the tensor-to-scalar ratio, $r < 0.036$ [3], we can constrain the Hubble scale during inflation as $H_I < 4.6 \times 10^{13}$ GeV.

We can check the parameter space for inflation in our model by writing Eqs. (23), (24), and (26) with $H_I^2 \simeq V_0/(3M_P^2)$ in the parametrization

$$n_s \simeq 1 + 2\eta_* \simeq 1 - \frac{|m_\phi^2|}{3H^2} \cos(\phi_*/f), \quad |m_\phi^2| = \frac{\Lambda^4}{f^2}, \quad (27)$$

$$N = \frac{\cos(\phi_*/f)}{|\eta_*|} \ln \left(\frac{\tan(\phi_c/(2f))}{\tan(\phi_*/(2f))} \right), \quad (28)$$

$$\frac{H_I}{f} = 2.9 \times 10^{-4} |\eta_* \tan(\phi_*/f)|, \quad (29)$$

together with Eq. (12). Equation (29) leads to the correlation between the axion decay constant and the Hubble scalar during inflation. Choosing $|\eta_*| = 0.033/2$ to get a consistent spectral index and $\cos(\phi_*/f) = 0.95$, we get $f \simeq 6.4 \times 10^5 H_I$. Thus, the decay constant for the pNGB inflaton is much larger than the Hubble scale, so the $U(1)$ global symmetry associated with the inflaton is broken during inflation. As we vary the Hubble scale during inflation [8], we can adjust f , $|m_\phi^2|$, and $\mu \sim m_\chi$ to maintain successful predictions for inflation while the waterfall fields remain safely decoupled during inflation.

B. Waterfall field dynamics

The waterfall field in the direction with $m_1^2 < 0$ starts rolling fast at $\phi = \phi_c$ and develops a nonzero background field. Then, the effective inflaton mass squared from $\frac{\partial^2 V}{\partial \phi^2}$ is modified to

$$m_{\phi,\text{eff}}^2 = -\frac{\Lambda^4}{f^2} \cos\left(\frac{\langle \phi \rangle}{f}\right) + \frac{\mu^2}{8f^2} (\langle \chi_1^2 \rangle - \langle \chi_2^2 \rangle) \sin\left(\frac{\langle \phi \rangle}{2f}\right), \quad (30)$$

where $\langle \rangle$ denotes the background field values. As a result, the inflaton settles down to a stable minimum near $\phi/f = \pi$, which is the common minimum for the inflaton potential and the waterfall-induced potential. On the other hand, the waterfall field masses are of order $\mu \sim m_\chi$ even after inflation ends, as will be shown below.

After inflation ends, we consider the post-inflation dynamics using the Boltzmann equations for scalar fields and the radiation energy density ρ_R ,

$$\ddot{\phi} + 3H\dot{\phi} = -\Gamma_\phi \dot{\phi} + \frac{\Lambda^4}{f} \sin\left(\frac{\phi}{f}\right) + \frac{\mu^2}{4f} \cos\left(\frac{\phi}{2f}\right) (\chi_1^2 - \chi_2^2), \quad (31)$$

$$\begin{aligned} \ddot{\chi}_1 + 3H\dot{\chi}_1 &= -\Gamma_{\chi_1} \dot{\chi}_1 + \mu^2 \sin\left(\frac{\phi}{2f}\right) \chi_1 - m_\chi^2 \chi_1 \\ &\quad - \alpha^2 \chi_2 - \lambda_\chi \chi_1^3 - \bar{\lambda}_\chi \chi_1 \chi_2^2, \end{aligned} \quad (32)$$

$$\begin{aligned} \ddot{\chi}_2 + 3H\dot{\chi}_2 &= -\Gamma_{\chi_2} \dot{\chi}_2 - \mu^2 \sin\left(\frac{\phi}{2f}\right) \chi_2 - m_\chi^2 \chi_2 \\ &\quad - \alpha^2 \chi_1 - \lambda_\chi \chi_2^3 - \bar{\lambda}_\chi \chi_1^2 \chi_2, \end{aligned} \quad (33)$$

$$\dot{\rho}_R + 4H\rho_R = \Gamma_\phi \dot{\phi}^2 + \Gamma_{\chi_1} \dot{\chi}_1^2 + \Gamma_{\chi_2} \dot{\chi}_2^2, \quad (34)$$

and the Friedmann equation,

$$H^2 = \frac{\rho_I + \rho_R}{3M_P^2}, \quad (35)$$

where ρ_I is the sum of energy densities for the inflaton and the waterfall fields, given by

$$\rho_I = \frac{1}{2} \dot{\phi}^2 + \frac{1}{2} \dot{\chi}_1^2 + \frac{1}{2} \dot{\chi}_2^2 + V. \quad (36)$$

Here, we maintain the homogeneity for scalar fields in space, but quantum fluctuations can give rise to nontrivial momentum modes of scalar fields during preheating or nonperturbative reheating, as will be discussed in the next section.

During the waterfall transition, the effective masses for the Higgs fields and the waterfall fields vary with time due to their couplings. We set the waterfall field χ_2 to zero at the

onset of the waterfall transition. Then, we find that the effective masses for the Higgs field and the waterfall field χ_2 take the following simple forms:

$$m_{H,\text{eff}}^2 = m_{H,0}^2 + \kappa_1 \chi_1^2(t), \quad (37)$$

$$m_{\chi_2,\text{eff}}^2 = m_{\chi_2,0}^2 + \bar{\lambda}_\chi \chi_1^2(t), \quad (38)$$

where $m_{H,0}^2, m_{\chi_2,0}^2$ are the squared bare masses, being independent of the field value of χ_1 .

C. Vacuum structure

We discuss the vacuum structure for the inflaton and the waterfall fields.

In the presence of a separate Z'_2 symmetry for χ_2 , which sets $\alpha = \beta = \gamma = \lambda'_\chi = 0$ in the waterfall sector potential, the vacuum structure gets simplified due to the unique minimum of the potential at $\langle \phi \rangle = \pi f$, $\langle \chi_1 \rangle = v_\chi$, and $\langle \chi_2 \rangle = 0$, with

$$v_\chi = \sqrt{\frac{\mu^2 - m_\chi^2}{\lambda_\chi}} \equiv \sqrt{\frac{m_1^2}{\lambda_\chi}}. \quad (39)$$

Then, the cosmological constant during inflation can be fine-tuned to the observed value in the true vacuum, if

$$V_0 - \Lambda^4 - \frac{1}{4} \lambda_\chi v_\chi^4 \simeq 0, \quad (40)$$

thus constraining the parameters of the waterfall fields. We note that in the situation where there is no Z'_2 symmetry [8], $\alpha \neq 0$ gives rise to a nonzero VEV for the waterfall field χ_2 , so, in general, the Z_2 symmetry is broken in the vacuum because $\langle \chi_1 \rangle \neq \langle \chi_2 \rangle$. Henceforth, we focus on the case with the Z'_2 symmetry for reheating and dark matter production.

There might be a concern regarding the domain-wall problem in our model, because the Z_2 symmetry for the waterfall fields is broken spontaneously in the vacuum. Namely, the vacuum A with $\langle \phi \rangle = \pi f$, $\langle \chi_1 \rangle = v_\chi$, and $\langle \chi_2 \rangle = 0$ is degenerate in energy with the vacuum B with $\langle \phi \rangle = -\pi f$, $\langle \chi_1 \rangle = 0$, and $\langle \chi_2 \rangle = v_\chi$. However, the inflaton direction is chosen to take positive values during the hybrid inflation and the Universe evolves only to the vacuum A through the waterfall transition, as discussed above. Thus, domain walls could be formed in the entire space, but the regions evolving into the vacuum B are beyond the Hubble horizon during the hybrid inflation and remain so at present, so there is no observable signature of the domain walls in the current Universe. As will be discussed later, the reheating temperature is smaller than the tachyonic mass of the waterfall field, the Z_2 symmetry is not restored, and a domain-wall problem does not occur even after reheating.

Here we comment on the constraints on the parameters of the waterfall fields from the vacuum structure. For $V_0 \gg \Lambda^4$, Eqs. (39) and (40) give rise to $4V_0/\lambda_\chi = v_\chi^4 = m_1^4/\lambda_\chi^2$. Then, the quartic coupling and the VEV for the waterfall fields are related to the dimensional parameters of the inflation as follows:

$$\lambda_\chi = \frac{m_1^4}{4V_0} = 1.4 \times 10^{-20} \left(\frac{m_1}{100H_I} \right)^4 \left(\frac{H_I}{10^5 \text{ GeV}} \right)^2, \quad (41)$$

$$v_\chi = \sqrt{\frac{4V_0}{m_1^2}} = 0.035 M_P \left(\frac{100H_I}{m_1} \right). \quad (42)$$

Therefore, since $H_I \lesssim 1.6 \times 10^{10}$ GeV for $f \lesssim 10^{16}$ GeV, the waterfall self-coupling λ_χ is smaller than about 10^{-10} for $\mu \gtrsim 100H_I$, and the VEV of the waterfall field v_χ is not far from the Planck scale.

Next, expanding around the VEV by $\phi = v_\phi + a$ and the waterfall fields as $\chi_1 = v_\chi + \tilde{\chi}_1$, we obtain the inflaton mass and the mass eigenvalues for the waterfall fields in the true vacuum as

$$m_a^2 = \frac{1}{f^2} \left(\Lambda^4 + \frac{1}{8} \mu^2 v_\chi^2 \right), \quad (43)$$

$$\begin{aligned} m_{\tilde{\chi}_1}^2 &= 2\lambda_\chi v_\chi^2 \\ &= 2(\mu^2 - m_\chi^2), \end{aligned} \quad (44)$$

$$\begin{aligned} m_{\chi_2}^2 &= \mu^2 + m_\chi^2 + \bar{\lambda}_\chi v_\chi^2 \\ &= \mu^2 + m_\chi^2 + \frac{\bar{\lambda}_\chi}{\lambda_\chi} (\mu^2 - m_\chi^2). \end{aligned} \quad (45)$$

We also note that the vacuum stability for the waterfall field potential requires $\lambda_\chi > 0$ and $\lambda_\chi + \bar{\lambda}_\chi > 0$ for $\bar{\lambda}_\chi < 0$.

We find that the inflaton mass receives a tree-level correction due to the waterfall field coupling. Using $|\eta_*| = \Lambda^4 \cos(\phi_*/f)/(f^2 H_I^2) = 0.033/2$, with $\cos(\phi_*/f) = 0.95$ at horizon exit, $f = 6.4 \times 10^5 H_I$, and $r \equiv \mu/m_\chi \gtrsim 1$, we can rewrite the effective inflaton mass as

$$m_a^2 = 0.0495 \frac{H_I^2}{\cos(\phi_*/f)} + (3 \times 10^{-9}) \left(\frac{r^2}{r^2 - 1} \right) \left(\frac{m_1}{100H_I} \right)^2 v_\chi^2. \quad (46)$$

Thus, as compared to the tachyonic mass for the waterfall field, we recall that $m_1^2 = \lambda_\chi v_\chi^2$, with $\lambda_\chi \lesssim 10^{-10}$, so the effective inflaton mass is much heavier than that of the waterfall fields. Therefore, the inflaton rapidly settles down to the minimum of the potential, so it does not influence the reheating dynamics with the waterfall fields. It is also possible to reheat the Universe from the inflaton energy density in the presence of interactions between the inflaton

and the SM particles, but reheating is dominated by the waterfall fields because $V_0 \gg \Lambda^4$.

For $m_{\tilde{\chi}_1} < 2m_{\chi_2}$, namely, for $(1 + 2\alpha_X)(\mu/m_\chi)^2 + 3 - 2\alpha_X < 0$, with $\alpha_X = \bar{\lambda}_X/\lambda_\chi$, the waterfall field $\tilde{\chi}_1$ could not decay into a χ_2 pair. This is the case in most of the parameter space where $\mu > m_\chi$ (waterfall condition) and $\alpha_X > -1$ (vacuum stability), so dark matter χ_2 is not produced from the decay of the waterfall field $\tilde{\chi}_1$. However, as will be shown below, dark matter χ_2 can still be produced abundantly during preheating.

Moreover, we find the leading interaction terms between the inflaton a , the mass eigenstates of the waterfall fields $\hat{\chi}_{1,2}$, and the Higgs boson h as follows:

$$\mathcal{L}_{\text{int}} = \frac{\mu^2}{8f^2} v_\chi a^2 \tilde{\chi}_1 + \frac{\mu^2}{16f^2} a^2 (\tilde{\chi}_1^2 - \tilde{\chi}_2^2) - \bar{\lambda}_\chi v_\chi \tilde{\chi}_1 \tilde{\chi}_2^2 - \kappa_1 v_\chi \tilde{\chi}_1 h^2 + \dots \quad (47)$$

Thus, we find that the inflation has no quadratic divergent mass correction thanks to the Z_2 symmetry. The logarithmic radiative corrections to the inflaton mass are present due to the cubic interactions in the first line of Eq. (47). We note that the decay modes, $\tilde{\chi}_1 \rightarrow aa, \chi_2 \chi_2$, are kinematically blocked in most of the parameter space, but $\tilde{\chi}_1 \rightarrow hh$ is open for reheating.

IV. REHEATING AND DARK MATTER PRODUCTION

We first discuss the preheating effects from the waterfall transition and the reheating from the perturbative decay of the waterfall field. Then, we show the time evolution of the radiation energy density and determine the maximum temperature and reheating temperature. We apply the results to obtain the relic density for dark matter.

A. Preheating

After the end of inflation, the equations of motion for scalars, $\psi = H, \chi_2$, can be written in terms of the rescaled field, $\varphi = a\psi$, as follows:

$$\varphi'' - \partial_i^2 \varphi + \left(m_{\psi,\text{eff}}^2 a^2 + (6\zeta_\psi - 1) \frac{a''}{a} \right) \varphi = 0, \quad (48)$$

where ζ_ψ is the nonminimal coupling of the scalar field ψ and we define the conformal time $\eta = \int dt/a(t)$, with $a(t)$ being the scale factor. In the case with $\zeta_\psi = \frac{1}{6}$, we get the total number density of produced particles at the end of the waterfall transition as

$$n_\psi = \frac{1}{2\pi^2} \int_0^\infty dk k^2 n_k^\psi, \quad (49)$$

where

$$n_k^\psi = -\frac{g_\psi}{2} + \frac{1}{2\omega_k} (|v'_k|^2 + \omega_k^2 |v_k|^2), \quad \omega_k^2 = k^2 + m_{\psi,\text{eff}}^2. \quad (50)$$

Here, v_k is the mode function for the scalar field, and g_ψ is the number of degrees of freedom for $\psi = H, \chi_2$. For $\zeta_\psi \neq \frac{1}{6}$, the Hubble expansion also affects the evolution of the scalar field.

We take the effective time-dependent scalar masses due to the waterfall transition [10] as

$$m_{\psi,\text{eff}}^2(t) = m_{\psi,0}^2 + \frac{1}{4} c_\psi v_\chi^2 (1 + \tanh \lambda(t - t_*))^2, \quad (51)$$

where $m_{\psi,0}^2$ are the bare masses and c_ψ are the couplings of the waterfall field χ_1 , given by $c_\psi = \kappa_1 \bar{\lambda}_\chi$ for $\psi = H, \chi_2$, respectively. Here, λ is the strength of the waterfall transition, given by $\lambda = m_1/2$, with $m_1 = \sqrt{\lambda_\chi} v_\chi$ being the tachyonic mass of the waterfall field χ_1 . $t_* \simeq \ln(32\pi^2/\lambda_\chi)/(2m_1)$ is the duration time of the waterfall transition [10], which is given by $t_* \simeq 14/m_1 - 26/m_1$ for $\lambda_\chi = 10^{-20} - 10^{-10}$. As $m_1 \gg H_{\text{end}}$, the waterfall transition takes place in less than one Hubble time and finishes rapidly. Thus, the Hubble expansion can be ignored during the waterfall transition, allowing us to set the scale factor to $a = 1$, so the situation does not change even for $\zeta_\psi \neq \frac{1}{6}$.

For a scalar field ψ with the effective mass given in Eq. (51), and following the general formalism for particle production in Refs. [11–13], we obtain the number density of produced particles with momentum k as

$$n_k^\psi = \frac{\cosh(\pi(w_{\psi,2} - w_{\psi,1})/\lambda) + \cosh(2\pi\delta)}{2 \sinh(\pi\omega_{\psi,1}/\lambda) \sinh(\pi\omega_{\psi,2}/\lambda)}, \quad (52)$$

where $w_{\psi,1}^2 = k^2 + m_{\psi,0}^2$, $w_{\psi,2}^2 = k^2 + m_{\psi,0}^2 + c_\psi v_\chi^2$, and $\delta = \frac{1}{2} \sqrt{\frac{c_\psi v_\chi^2}{\lambda^2} - 1}$. Therefore, we obtain the energy density of the produced particles at the end of the waterfall transition as

$$\rho_\psi(t_*) = \frac{g_\psi}{2\pi^2} \int_0^\infty dk k^2 n_k^\psi w_{\psi,2}. \quad (53)$$

As a consequence, the ratio of the produced energy density to the initial vacuum energy density, $V_0 \simeq \frac{1}{4} \lambda_\chi v_\chi^4 = \frac{m_1^4}{4\lambda_\chi}$, is given by

$$\frac{\rho_\psi(t_*)}{V_0} = \frac{2g_\psi \lambda_\chi}{\pi^2} \int_0^\infty d\kappa \kappa^2 n_k^\psi \sqrt{\kappa^2 + \frac{m_{\psi,0}^2}{m_1^2} + \alpha_\psi}, \quad (54)$$

with $\kappa = k/m_1$ and $\alpha_\psi = c_\psi/\lambda_\chi$. In order to compare our results with lattice calculations [10], for $m_{\psi,0} = 0$ we quote

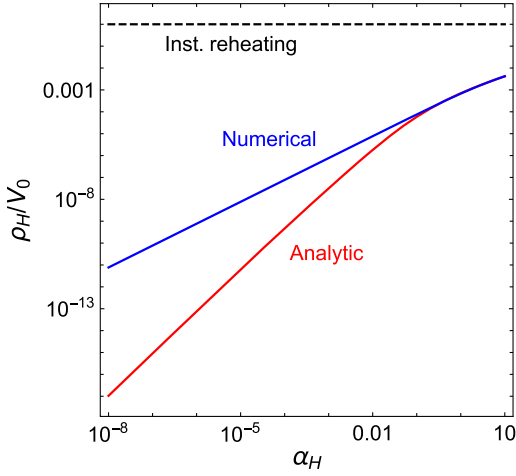


FIG. 1. Analytic and numerical solutions for ρ_H/V_0 from preheating as a function of $\alpha_H = \kappa_1/\lambda_\chi$ (red and blue lines, respectively).

the numerical solution for $\frac{\rho_\psi(t_*)}{V_0}$ in terms of a fitting function, $f(\alpha, \gamma) = \sqrt{\alpha + \gamma^2} - \gamma$ [10], as follows:

$$\frac{\rho_\psi(t_*)}{V_0} = 2 \times 10^{-3} g_\psi \lambda_\chi f(\alpha_\psi, 1.3). \quad (55)$$

Similarly, the numerical result for the number density at the waterfall transition is given by [10]

$$n_\psi(t_*) = 10^{-3} g_\psi m_1^3 f(\alpha_\psi, 1.3) / \alpha_\psi. \quad (56)$$

In Fig. 1 we depict the analytic and numerical results for ρ_H/V_0 for the Higgs as a function of $\alpha_H = \kappa_1/\lambda_\chi$ as red and blue lines, respectively. We set the bare Higgs mass to $m_{H,0} = 0$. The analytic result is based on the formula in Eq. (54), while the numerical result is taken from Eq. (55). For $\alpha_H \gtrsim 0.1$, the analytic and numerical results agree. The black dashed line corresponds to the case of instantaneous reheating.

B. Reheating completion

At the end of preheating, the waterfall fields reach the minimum of the scalar potential and start oscillating around it. Then, if preheating is not efficient, we can determine the reheating temperature from the perturbative decay of the waterfall field condensate into an SM Higgs pair as

$$T_{\text{RH}} = \left(\frac{90}{\pi^2 g_{\text{RH}}} \right)^{1/4} \sqrt{M_P \Gamma_{\chi_1 \rightarrow hh}}, \quad (57)$$

where g_{RH} is the number of relativistic degrees of freedom at reheating completion and $\Gamma_{\chi_1 \rightarrow hh}$ is the partial decay rate for $\chi_1 \rightarrow hh$.

Expanding the waterfall field as $\chi_1(t) = v_\chi + \chi_c(t)$, with $\chi_c(t)$ being the waterfall condensate, we note that the total decay rate of the waterfall condensate is

$$\Gamma_{\chi_1} = \Gamma_{\chi_1 \rightarrow hh} + \Gamma_{\chi_1 \rightarrow \chi_2 \chi_2}, \quad (58)$$

with

$$\Gamma_{\chi_1 \rightarrow hh} = \frac{\kappa_1^2 v_\chi^2}{2\pi m_{\chi_1}} \sqrt{1 - \frac{4m_H^2}{m_{\chi_1}^2}}, \quad (59)$$

$$\Gamma_{\chi_1 \rightarrow \chi_2 \chi_2} = \frac{\bar{\lambda}_\chi^2 v_\chi^2}{2\pi m_{\chi_1}} \sqrt{1 - \frac{4m_{\chi_2}^2}{m_{\chi_1}^2}}. \quad (60)$$

Then, ignoring the Higgs and χ_2 masses, we obtain the approximate reheating temperature as

$$T_{\text{RH}} \simeq \left(\frac{90}{\pi^2 g_{\text{RH}}} \right)^{1/4} \left(\frac{\kappa_1^2}{4\pi \lambda_\chi} \right)^{1/2} \sqrt{M_P m_{\chi_1}}. \quad (61)$$

Therefore, for $\Gamma_{\chi_1} \ll H_I \sim m_{\chi_1}$, namely, $\kappa_1^2 \ll 4\pi \lambda_\chi$, and taking $H_I \lesssim 1.6 \times 10^{10}$ GeV for $f \lesssim 10^{16}$ GeV, we get the reheating temperature as $T_{\text{RH}} \ll 10^{14}$ GeV.

More concretely, from Eq. (61) with $\lambda_\chi = m_1^4 / (12H_I^2 M_P^2)$ in Eq. (41), we can rewrite the reheating temperature as

$$T_{\text{RH}} \simeq 0.04 \alpha_H m_1 \left(\frac{100}{g_{\text{RH}}} \right)^{1/4} \left(\frac{m_1}{M_P} \right)^{1/2} \left(\frac{m_1}{H_I} \right). \quad (62)$$

Thus, taking $m_1 \sim 100H_I \ll M_P$, with $H_I \lesssim 4.6 \times 10^{13}$ GeV [from the bound on the tensor-to-scalar ratio below Eq. (26)], for $\alpha_H \lesssim 10$, we find that the reheating temperature is smaller than the tachyonic mass of the waterfall field, so the domain-wall problem will not occur even after reheating, as mentioned in Sec. III C.

The waterfall transition takes place faster than the Hubble expansion, so preheating is instantaneous. But, if the reheating during the waterfall oscillation is sizable and it is not instantaneous, the number of e -foldings required to solve the horizon problem [14,15] is modified to

$$N = 61.1 + \Delta N - \ln \left(\frac{V_0^{1/4}}{H_k} \right) - \frac{1}{12} \ln \left(\frac{g_{\text{RH}}}{106.75} \right), \quad (63)$$

where the correction to the number of e -foldings due to the noninstantaneous reheating is given by

$$\Delta N = \frac{1}{12} \left(\frac{3w-1}{w+1} \right) \ln \left(\frac{45\rho_{\chi_1}(t_*)}{\pi^2 g_{\text{RH}} T_{\text{RH}}^4} \right). \quad (64)$$

Here, $\rho_{\chi_1}(t_*) = V_0 - \rho_R(t_*)$ is the energy density of the waterfall field at the end of the waterfall transition and w is the equation of state for the waterfall condensate.

Here, H_k is the Hubble parameter evaluated at the horizon exit for the Planck pivot scale, $k = 0.05 \text{ Mpc}^{-1}$, and w is the averaged equation of state during reheating. Then, taking $w = 0$ for $V_0 \gtrsim \rho_R(t_*)$ and $g_{\text{RH}} = 106.75$ in Eq. (64), we obtain the number of e -foldings as

$$N = 51.3 - \frac{1}{3} \ln \left(\frac{H_I}{1.6 \times 10^{10} \text{ GeV}} \right) - \frac{1}{12} \ln \left(1 - \frac{\rho_R(t_*)}{V_0} \right) + \frac{1}{3} \ln \left(\frac{T_{\text{RH}}}{10^{14} \text{ GeV}} \right). \quad (65)$$

As a result, we conclude that there is a wide range of the parameter space for a successful inflation, and a sufficiently large reheating temperature is achieved due to the decay of the waterfall field.

C. Time evolution of radiation energy density

Here we discuss the time evolution of the waterfall and radiation energy densities after preheating and determine the reheating temperature.

After preheating, we consider the Boltzmann equations in the presence of the coherent oscillation of the waterfall field as follows:

$$\dot{\rho}_R + 4H\rho_R = \Gamma_{\chi_1 \rightarrow hh} \rho_{\chi_1}, \quad (66)$$

$$\dot{\rho}_{\chi_1} + 3H\rho_{\chi_1} = -\Gamma_{\chi_1} \rho_{\chi_1}, \quad (67)$$

with

$$H^2 = \frac{\rho_R + \rho_{\chi_1}}{3M_P^2}. \quad (68)$$

We take the initial condition for the waterfall energy density at preheating as $\rho_{\chi_1}(t_*) = V_0 - \rho_R(t_*)$, where $\rho_R(t_*) = \rho_H$ is the radiation energy density from preheating. For a constant decay rate, $\Gamma_{\chi_1} \simeq \Gamma_{\chi_1 \rightarrow hh}$, we obtain the analytic solutions to the above Boltzmann equations as [16]

$$\rho_{\chi_1}(t) = \rho_{\chi_1}(t_*) \left(\frac{a(t)}{a_*} \right)^{-3} e^{-\Gamma_{\chi_1}(t-t_*)}, \quad (69)$$

$$\rho_R(t) = \rho_{\chi_1}(t_*) \left(\frac{a(t)}{a_*} \right)^{-4} \left[\frac{\rho_R(t_*)}{\rho_{\chi_1}(t_*)} + \int_{u_*}^u \left(\frac{a(u)}{a_*} \right) e^{u_* - u} du \right]. \quad (70)$$

Here, $u = \Gamma_{\chi_1} t$ and $u_* = \Gamma_{\chi_1} t_*$.

Combining Eq. (68) and the effective continuity equation for the total energy density, $\rho = \rho_{\chi_1} + \rho_R$, given by

$$\dot{\rho} + 3H\rho(1 + w(t)) = 0, \quad (71)$$

with $w(t)$ being the effective equation of state, we find the total energy density as

$$\rho(t) = V_0 \left(1 + \sqrt{\frac{3}{4}} V_0 (1 + \bar{w}) \frac{t - t_*}{M_P} \right)^{-2}, \quad (72)$$

where

$$\bar{w}(t) = \frac{1}{t - t_*} \int_{t_*}^t dt' w(t'). \quad (73)$$

Here we used $\rho_{\chi_1} + \rho_R \simeq V_0$ at the waterfall transition. Then, for a slowly varying \bar{w} , we also obtain the scale factor as a function of time,

$$\frac{a(t)}{a_*} \simeq \left(1 + \sqrt{\frac{3}{4}} V_0 (1 + \bar{w}) \frac{t - t_*}{M_P} \right)^{\frac{2}{3(1+\bar{w})}}. \quad (74)$$

Setting $\bar{w} = 0$ for the waterfall field oscillation near the quadratic potential and using the results in Eqs. (70) and (74), we get the total radiation energy density after preheating as follows:

$$\rho_R(t) = \rho_{\chi_1}(t_*) \left(1 + \frac{v}{A} \right)^{-8/3} \times \left[\frac{\rho_R(t_*)}{\rho_{\chi_1}(t_*)} + \int_0^v \left(1 + \frac{v'}{A} \right)^{2/3} e^{-v'} dv' \right], \quad (75)$$

where $v \equiv \Gamma_{\chi_1}(t - t_*)$ and

$$A = \frac{\Gamma_{\chi_1}}{m_{\chi_1}} \left(\frac{3}{4} \frac{V_0}{m_{\chi_1}^2 M_P^2} \right)^{-1/2} = 4 \sqrt{\frac{2}{3}} \frac{\Gamma_{\chi_1}}{m_{\chi_1}} \left(\frac{v_{\chi}}{M_P} \right)^{-1}. \quad (76)$$

Here we used $V_0 = \frac{m^4}{4\lambda_{\chi}}$ and $m_1^2 = \lambda_{\chi} v_{\chi}^2 = m_{\chi_1}^2/2$ in the second line of Eq. (76).

In Fig. 2 we depict the time evolution of ρ_{χ_1}, ρ_R as functions of $\Gamma_{\chi_1}(t - t_*)$ (blue and red solid lines, respectively) for $H_I = 10^6, 10^{10} \text{ GeV}$ in the left and right plots. We find that the reheating temperature T_{RH} is determined from $\rho_R = \rho_{\chi_1}$, for which $\Gamma_{\chi}(t - t_*) \sim 1$. Thus, the results are consistent with the identification of the reheating temperature by Eq. (57) with $\Gamma_{\chi_1} \simeq \Gamma_{\chi_1 \rightarrow hh}$.

The second term from reheating in Eq. (75) is maximized at $v_{\text{max}} = \Gamma_{\chi_1}(t_{\text{max}} - t_*) = 0.80A$, resulting in the maximum radiation energy,

$$\rho_R(t_{\text{max}}) = 1.8^{-8/3} (\rho_R(t_*) + 1.0A\rho_{\chi_1}(t_*)). \quad (77)$$

Therefore, for $\rho_R(t_*) \lesssim V_0$ and $\rho_{\chi_1}(t_*) \simeq V_0$, we get the maximum ratio of reheating to preheating contributions to the radiation energy density as

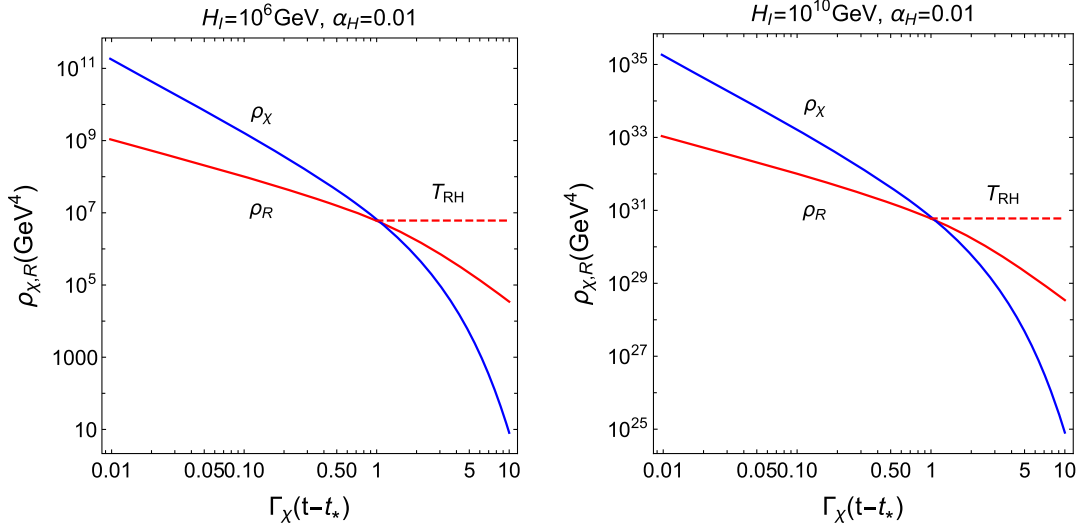


FIG. 2. ρ_χ, ρ_R as functions of $\Gamma_{\chi_1}(t-t_*)$ (blue and red solid lines, respectively). Red dashed lines correspond to the reheating completion. We take $\alpha_H = 0.01$ and $m_1 = 100H_I$ for both plots, and $H_I = 10^6, 10^{10}$ GeV in the left and right plots, respectively.

$$R_{\text{th}} \equiv \frac{1.0A\rho_{\chi_1}(t_*)}{\rho_R(t_*)} \simeq 1600 \frac{\Gamma_{\chi_1}/m_{\chi_1}}{\lambda_\chi f(\alpha_H, 1.3)} \left(\frac{v_\chi}{M_P}\right)^{-1} \simeq 130 \frac{\alpha_H^2}{f(\alpha_H, 1.3)} \left(\frac{v_\chi}{M_P}\right)^{-1}. \quad (78)$$

Here we used Eq. (76) and the numerical result for preheating with the Higgs coupling, $\alpha_H = \kappa_1/\lambda_\chi$, in Eq. (55), and took Eq. (58) in the second equality. Thus, from Eq. (78) and with Eq. (42), we find that

$$R_{\text{th}} \simeq 3700 \frac{\alpha_H^2}{f(\alpha_H, 1.3)} \left(\frac{m_1}{100H_I}\right). \quad (79)$$

In Fig. 3 we show the fraction of the radiation energy in the waterfall energy density at the end of inflation, ρ_R/V_0 , as a function of $\alpha_H = \kappa_1/\lambda_\chi$, for preheating (blue solid line) and the decay of the waterfall field (purple dashed line). For comparison, we also show the case for instantaneous reheating, $\rho_R/V_0 = 1$ (black dashed line). Then, for $m_1 = 100H_I$, we get $R_{\text{th}} \gtrsim 1$ for $\alpha_H \gtrsim 2.6 \times 10^{-5}$, so the decay of the waterfall field is dominant for reheating.

For $R_{\text{th}} \gtrsim 1$ and $A \ll v \ll 1$, we can approximate Eq. (75) to

$$\rho_R \simeq \frac{4}{5} (\Gamma_{\chi_1} M_P)^2 v^{-1} = \frac{\pi^2}{30} g_* T^4 \quad (80)$$

and rewrite the scale factor in Eq. (74) as a function of the radiation temperature T as

$$\left(\frac{a}{a_*}\right)^3 \simeq \left(\frac{v}{A}\right)^2 = \left(\frac{24\Gamma_{\chi_1}^2 M_P^2}{g_* \pi^2 A T^4}\right)^2. \quad (81)$$

So, choosing $T = T_{\text{RH}}$ in the above result, we can take into account the redshift factor from the waterfall transition to the reheating completion.

In Fig. 4 we show the maximum and reheating temperatures as functions of $\alpha_H = \kappa_1/\lambda_\chi$ (red solid and dashed lines, respectively). We chose $H_I = 10^6, 10^8, 10^{10}$ GeV from left to right. The lower bound on the reheating temperature for BBN is set to $T_{\text{BBN}} = 10$ MeV (blue dashed lines) and the black dashed lines correspond to instantaneous reheating, for comparison. Consequently, for a relatively small Hubble scale as in the left plot, the waterfall coupling to the Higgs field should be sizable for a successful reheating; for instance, $\alpha_H \gtrsim 5 \times 10^{-6}$ for

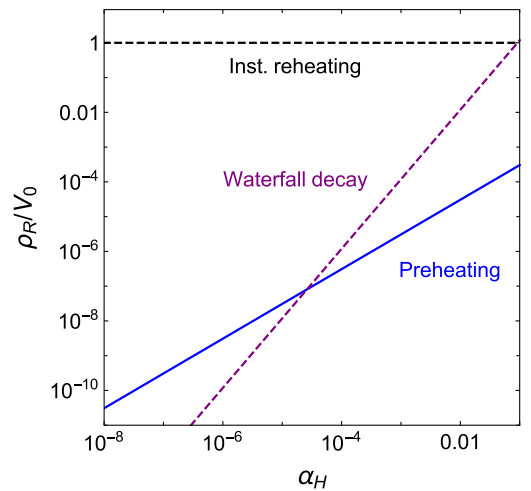


FIG. 3. ρ_R/V_0 as a function of $\alpha_H = \kappa_1/\lambda_\chi$, from preheating (blue solid line) and its maximum value from the decay of the waterfall field (purple dashed line). We take $m_1 = 100H_I$. The black dashed line corresponds to the instantaneous reheating.

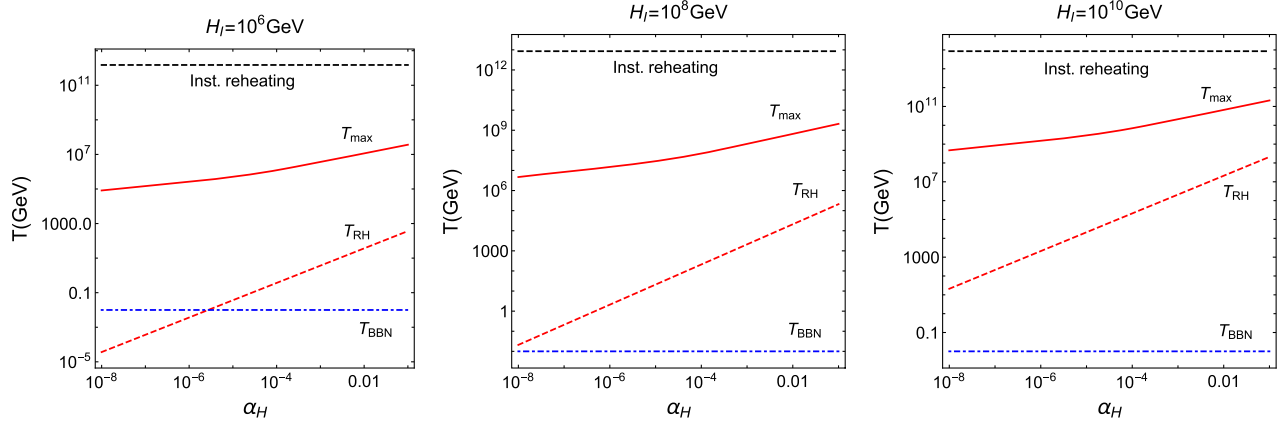


FIG. 4. Maximum and reheating temperatures as functions of $\alpha_H = \kappa_1/\lambda_\chi$ (red solid and dashed lines, respectively) for $H_I = 10^6, 10^8, 10^{10}$ GeV from left to right. We take $m_{\psi,0} = 0$ and $m_1 = 100H_I$. Black dashed lines correspond to the instantaneous reheating and blue dot-dashed lines correspond to $T_{RH} = 10$ MeV, which is the lower bound from BBN.

$H_I = 10^6$ GeV. However, for a high Hubble scale, as in the middle and right plots, small waterfall couplings can be compatible with BBN, for which the preheating effect as shown in Fig. 3 becomes important for reheating.

D. Dark matter production

If the Z'_2 symmetry for the waterfall field χ_2 is unbroken in the vacuum, the waterfall field χ_2 can be a dark matter candidate. Dark matter can be produced from preheating, but there is no production from the decay of the waterfall field χ_1 due to the kinematic blocking, namely, $m_{\tilde{\chi}_1} < 2m_{\chi_2}$, from Eqs. (44) and (45).

From the result in Eq. (55), preheating leads to the number density for dark matter $X = \chi_2$ as

$$n_X(t_*) = 10^{-3} m_1^3 f(\alpha_X, 1.3) / \alpha_X, \quad (82)$$

with $\alpha_X = \bar{\lambda}_\chi / \lambda_\chi$. Then, the number density produced from preheating becomes redshifted at the reheating temperature as follows:

$$n_X^{\text{pre}}(T_{RH}) = \left(\frac{a_*}{a(T_{RH})} \right)^3 n_X(t_*) = \left(\frac{g_* \pi^2 A T_{RH}^4}{24 \Gamma_{\chi_1}^2 M_P^2} \right)^2 n_X(t_*), \quad (83)$$

where Eq. (81) at the reheating temperature is used in the second equality. As a result, the relic density for dark matter χ_2 at present is given by

$$\begin{aligned} \Omega_{\text{DM}} h^2 &= \frac{m_{\chi_2} n_X(t_0)}{\rho_c / h^2} \\ &= 5.9 \times 10^6 \left(\frac{n_X^{\text{pre}}(T_{RH})}{T_{RH}^3} \right) \left(\frac{m_{\chi_2}}{1 \text{ GeV}} \right). \end{aligned} \quad (84)$$

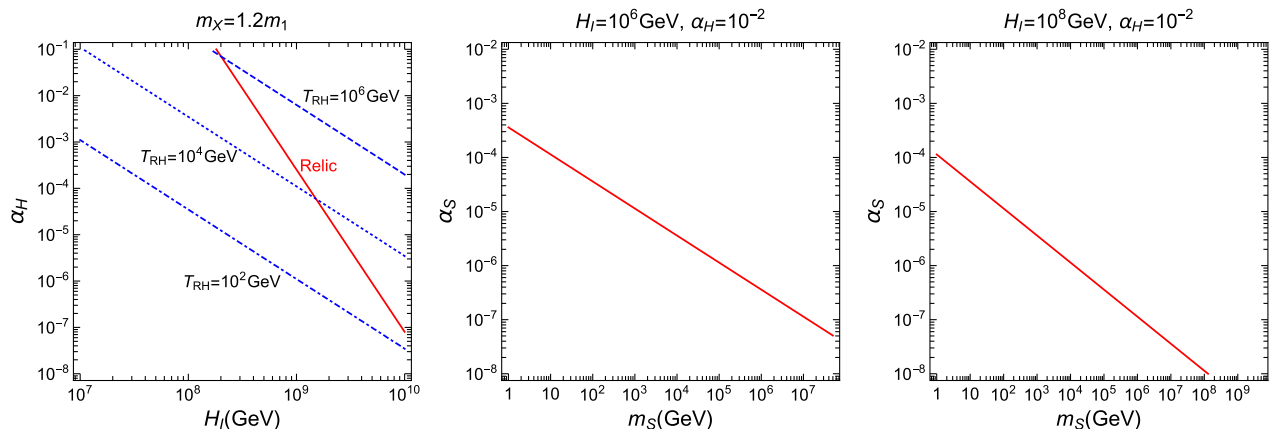


FIG. 5. Parameter space satisfying the relic density (red lines). Left: H_I vs α_H with the relic density from dark matter χ_2 . We choose $m_X = 1.2m_1$ and draw the with reheating temperature contours $T_{RH} = 10^2, 10^4, 10^6$ GeV (blue dashed, dotted, and dot-dashed lines, respectively). The results are insensitive to $\alpha_X = \bar{\lambda}_\chi / \lambda_\chi$ as long as $\alpha_X \lesssim \alpha_H$. Middle and right: m_S vs α_S with the relic density from dark matter S . We choose $\alpha_H = 10^{-2}$ for both plots, but $H_I = 10^6, 10^8$ GeV in the middle and right plots, respectively. We take $m_1 = 100H_I$ for all plots.

In the left plot of Fig. 5 we show the parameter space for H_I vs $\alpha_H = \kappa_1/\lambda_\chi$, satisfying the relic density for dark matter χ_2 (red line). We take the dark matter mass to be $m_\chi = 1.2m_1$ and $m_1 = 100H_I$. The results are insensitive to the dark matter coupling α_χ as long as $\alpha_\chi \lesssim \alpha_H$ because the numerical formula for the number density of dark matter in Eq. (82) does not depend much on α_χ . We also show the contours of the reheating temperature $T_{\text{RH}} = 10^2, 10^4, 10^6$ GeV (blue dashed, dotted, and dot-dashed lines, respectively). In this case, we find that the correct relic density can be achieved for $\alpha_H = 0.1\text{--}10^{-7}$ and $H_I = 2 \times 10^8\text{--}10^{10}$ GeV. Thus, we need a relatively high reheating temperature for the relic density.

Suppose that there is a real scalar dark matter S that does not participate in the waterfall transition, transforms by $S \rightarrow -S$ under the Z'_2 symmetry, and takes the following effective squared mass:

$$m_{S,\text{eff}}^2 = m_{S,0}^2 + \lambda_S \chi_1^2(t), \quad (85)$$

where $m_{S,0}^2$ is the squared bare mass and λ_S is the coupling between S and the waterfall field χ_1 . Then, S particles can be produced from not only preheating but also the decay of the waterfall field χ_1 . The Boltzmann equation for the dark matter density after preheating is given by

$$\dot{n}_S + 3Hn_S = 2B_{\chi_1} \Gamma_{\chi_1} \frac{\rho_{\chi_1}}{m_{\chi_1}}, \quad (86)$$

where B_{χ_1} is the decay branching ratio for $\chi_1 \rightarrow SS$. Then, solving the above Boltzmann equation with Eq. (57), we obtain the number density at the reheating temperature from the decay of the waterfall field χ_1 as [17]

$$n_S^{\text{decay}}(T_{\text{RH}}) = \frac{g_*(T_{\text{RH}})\pi^2 B_{\chi_1} T_{\text{RH}}^4}{18m_{\chi_1}}. \quad (87)$$

As a result, we obtain the relic density for the scalar dark matter S at present as follows:

$$\begin{aligned} \Omega_{\text{DM}} h^2 &= \frac{m_S n_S(t_0)}{\rho_c/h^2} \\ &= 5.9 \times 10^6 \left(\frac{n_S(T_{\text{RH}})}{T_{\text{RH}}^3} \right) \left(\frac{m_S}{1 \text{ GeV}} \right), \end{aligned} \quad (88)$$

where the total number density for dark matter is given by the sum of both the preheating and decay contributions,

$$n_S(T_{\text{RH}}) = n_S^{\text{pre}}(T_{\text{RH}}) + n_S^{\text{decay}}(T_{\text{RH}}). \quad (89)$$

Here $n_S^{\text{pre}}(T_{\text{RH}})$ is the preheating contribution, obtained from Eqs. (82) and (83) with α_χ being replaced by α_S .

In the middle and right plots of Fig. 5 we show the parameter space for m_S vs α_S , satisfying the correct relic

density for S in the case with $H_I = 10^6, 10^8$ GeV, respectively. We choose $\alpha_H = 10^{-2}$ and $m_1 = 100H_I$ for both plots. As a result, we find that dark matter with masses up to $m_S = 1\text{--}10^8$ GeV can be produced with a correct relic density for $10^{-4} \gtrsim \alpha_S \gtrsim 10^{-8}$.

V. CONCLUSIONS

We have explored the inflation and post-inflationary evolution of the Universe in the hybrid inflation with a pNGB boson inflaton and two waterfall scalar fields. The couplings between the inflaton and the waterfall fields were introduced for the graceful exit, but the Z_2 symmetry for the twin waterfall fields ensure that the quadratic divergent loop corrections to the inflaton potential are canceled, so the inflationary predictions of the hybrid inflation are maintained at the quantum level for a wide range of the parameter space.

The Z_2 symmetry is broken spontaneously in the vacuum when the inflaton and the waterfall fields settle down to the local minimum of the potential, but there is no domain-wall problem during inflation or after reheating because the domain walls could only form beyond the horizon of our Universe during inflation, and the Z_2 symmetry is not restored by reheating due to a low reheating temperature in our model.

We showed that the Z_2 -invariant couplings between the waterfall fields and the SM Higgs are responsible for the reheating process via preheating and the perturbative decay of the waterfall field. Thus, we achieved the post-inflationary Universe with a sufficiently large reheating temperature being compatible with BBN, depending on the Higgs coupling to the waterfall field. On the other hand, the inflaton receives a large mass in the Z_2 -breaking minimum, with a large VEV for the waterfall field that is larger than the VEV for the other waterfall field, so it rapidly settles down to the minimum of the inflaton potential without changing the results on reheating with the waterfall fields.

In the presence of an extra Z'_2 symmetry, one of the waterfall fields or another singlet scalar field becomes a dark matter candidate. Although the mass of the waterfall dark matter is constrained to be comparable to the other waterfall field by the Z_2 symmetry, we showed that the correct relic abundance for dark matter can be produced via preheating.

ACKNOWLEDGMENTS

We thank Seong Chan Park for interesting discussion on the subject. This work is supported in part by the Basic Science Research Program through the National Research Foundation of Korea (NRF) funded by the Ministry of Education, Science and Technology (NRF-2022R1A2C2003567 and NRF-2021R1A4A2001897).

- [1] A. H. Guth, *Phys. Rev. D* **23**, 347 (1981).
- [2] Y. Akrami *et al.* (Planck Collaboration), *Astron. Astrophys.* **641**, A10 (2020).
- [3] P. A. R. Ade *et al.* (BICEP and Keck Collaborations), *Phys. Rev. Lett.* **127**, 151301 (2021).
- [4] A. D. Linde, *Phys. Lett.* **129B**, 177 (1983).
- [5] J. H. Traschen and R. H. Brandenberger, *Phys. Rev. D* **42**, 2491 (1990); A. D. Dolgov and D. P. Kirilova, *Sov. J. Nucl. Phys.* **51**, 172 (1990); L. Kofman, A. D. Linde, and A. A. Starobinsky, *Phys. Rev. Lett.* **73**, 3195 (1994); *Phys. Rev. D* **56**, 3258 (1997); Y. Shtanov, J. H. Traschen, and R. H. Brandenberger, *Phys. Rev. D* **51**, 5438 (1995).
- [6] A. D. Linde, *Phys. Rev. D* **49**, 748 (1994);
- [7] G. N. Felder, L. Kofman, and A. D. Linde, *Phys. Rev. D* **64**, 123517 (2001).
- [8] H. M. Lee and A. G. Menkara, *Phys. Lett. B* **834**, 137483 (2022).
- [9] K. Deshpande, S. Kumar, and R. Sundrum, *J. High Energy Phys.* **07** (2020) 147.
- [10] J. Garcia-Bellido and E. Ruiz Morales, *Phys. Lett. B* **536**, 193 (2002).
- [11] E. W. Kolb, D. J. H. Chung, and A. Riotto, *AIP Conf. Proc.* **484**, 91 (1999); G. F. Giudice, M. Peloso, A. Riotto, and I. Tkachev, *J. High Energy Phys.* **08** (1999) 014; G. F. Giudice, I. Tkachev, and A. Riotto, *J. High Energy Phys.* **08** (1999) 009.
- [12] V. Mukhanov and S. Winitzki, *Introduction to Quantum Effects in Gravity* (Cambridge University Press, Cambridge, England, 2007).
- [13] C. W. Bernard and A. Duncan, *Ann. Phys. (N.Y.)* **107**, 201 (1977); N. D. Birrell and P. C. W. Davies, *Quantum Fields in Curved Space* (Cambridge University Press, Cambridge, England, 2012); M. Herranen, T. Markkanen, S. Nurmi, and A. Rajantie, *Phys. Rev. Lett.* **115**, 241301 (2015).
- [14] S. M. Choi and H. M. Lee, *Eur. Phys. J. C* **76**, 303 (2016).
- [15] S. Aoki, H. M. Lee, A. G. Menkara, and K. Yamashita, *J. High Energy Phys.* **05** (2022) 121.
- [16] J. Ellis, M. A. G. Garcia, D. V. Nanopoulos, K. A. Olive, and M. Peloso, *J. Cosmol. Astropart. Phys.* **03** (2016) 008; M. A. G. Garcia, Y. Mambrini, K. A. Olive, and M. Peloso, *Phys. Rev. D* **96**, 103510 (2017).
- [17] K. Kaneta, Y. Mambrini, and K. A. Olive, *Phys. Rev. D* **99**, 063508 (2019).